# Journal Pre-proof

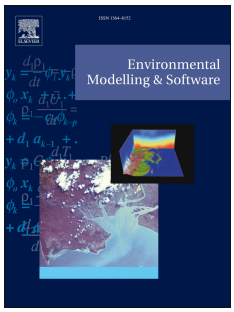


A python toolkit to monitor sandy shoreline change using high-resolution PlanetScope cubesats

Yarran Doherty, Mitchell D. Harley, Kilian Vos, Kristen D. Splinter

PII: S1364-8152(22)00212-2

DOI: https://doi.org/10.1016/j.envsoft.2022.105512

Reference: ENSO 105512

To appear in: *Environmental Modelling and Software*

Received Date: 18 February 2022

Revised Date: 22 August 2022

Accepted Date: 31 August 2022

Please cite this article as: Doherty, Y., Harley, M.D., Vos, K., Splinter, K.D., A python toolkit to monitor sandy shoreline change using high-resolution PlanetScope cubesats, *Environmental Modelling and Software* (2022), doi: https://doi.org/10.1016/j.envsoft.2022.105512.

# A Python toolkit to monitor sandy shoreline change using high-resolution PlanetScope cubesats

Yarran Doherty[1], Mitchell D. Harley[1], Kilian Vos[1], Kristen D. Splinter[1]

[1]Water Research Laboratory, School of Civil and Environmental Engineering, UNSW Sydney, 110 King Street, Manly Vale, NSW, 2093, Australia

Corresponding Author:
m.harley@unsw.edu.au

## *Abstract*

This study evaluates an emerging capability to monitor high spatial (pixel size = 3.7 m) and temporal (daily to sub-daily imagery) resolution coastal change using PlanetScope cubesats. A new toolkit (*CoastSat.PlanetScope*) is presented that enables users to map shorelines from PlanetScope imagery, using a workflow of image co-registration, segmentation, thresholding, shoreline detection and elevation correction. The toolkit is subsequently tested at Narrabeen-Collaroy Beach (SE Australia), evaluating combinations of shoreline detection indices, thresholding approaches and elevation correction. An optimal shoreline accuracy of 3.5 m (RMSE) is found for this coastline using the difference between the near-infrared and blue bands and a weighted peaks thresholding approach. A generic elevation correction model that considers tidal variability and wave setup at the shoreline is then proposed. With a growing archive of high-resolution imagery, PlanetScope presents enormous potential for enhanced coastline mapping of the coast and complements existing approaches using Landsat/Sentinel-2 imagery.


Keywords: coastal monitoring; remote sensing; extreme storms; Narrabeen; CoastSat

## *Software availability*

| | |
|---|---|
| **Software name**: | *CoastSat.PlanetScope* |
| **Developer**: | Yarran Doherty |
| **Year first official release**: | 2021 |
| **Hardware requirements**: | PC |
| **System requirements**: | Windows, Linux, Mac |
| **Program language**: | Python |
| **Program size**: | 18 MB |
| **Availability**: | https://github.com/ydoherty/CoastSat.PlanetScope |
| **License**: | GPL-3.0 |
| **Documentation**: | README in Github repository and guided example in Jupyter Notebook |
| Run times: | The data presented here was run a a 2013 MackBook Pro 8GB RAM with a 2.5 GHz Dual-Core Intel i5 processor. For the 1000 images downloaded (each image between 2 and 5mb) the total processing time was approximately 5 hours and as follows: 20 minutes for pre-processing (TOA conversion and masking); 2.5 hours for co-registration; 35 min for scene merging; 1 hr for image classification and 50 min for shoreline extraction. |

# 1. Introduction

The two-dimensional shoreline position is a fundamental metric in coastal engineering and coastal management (Boak and Turner, 2005; Luijendijk et al., 2018; Vousdoukas et al., 2020). Among other things, the shoreline position is a good proxy for the amount of beach sediment stored on the subaerial beach (Farris and List, 2007), the width of the dry beach for both recreational purposes (e.g., Silberman and Klock, 1988) and coastal habitats (e.g., Fish et al., 2008), and the amount of sand buffer needed for protection against extreme storm events (e.g., Harley et al., 2009; Plant and Stockdon, 2012). While time series of shoreline position can be obtained using *in-situ* instrumentation (Emery, 1961; Moore, 2000), mapping the shoreline position is increasingly undertaken using remote sensing (Splinter et al., 2018). This has historically comprised aerial photographs or photogrammetry (Romine and Fletcher, 2013) and, as technology has progressed, extended to other platforms such as ground-based video (Holman et al., 2003; Pianca et al., 2015), UAV (Pucino et al., 2021; Turner et al., 2016a), smartphones (Harley et al., 2019; Jaud et al., 2019) and satellites (Almeida et al., 2021; Pardo-Pascual et al., 2012; Vos et al., 2019b, Bishop-Taylor et al., 2021).

Providing global coverage, satellites are particularly appealing to monitoring coastline change and satellite-derived shoreline (or SDS) mapping has been the focus of recent research (e.g., Liu et al., 2017; Pardo-Pascual et al., 2012). Applications range from opportunistic, site-specific investigations (e.g. Ford, 2013) to global-scale studies of multi-decadal shoreline trends (e.g. Luijendijk et al., 2018; Mentaschi et al., 2018). The vast majority of studies involving satellite-derived shorelines to date have been based on the publicly-available Landsat and/or Sentinel-2 data (Almonacid-Caballer et al., 2016; Hagenaars et al., 2018; Pardo-Pascual et al., 2018, 2012, Mao et al., 2021). This has been in part driven by cloud computing resources, such as Google Earth Engine (Gorelick et al., 2017), that streamline data access to the vast Landsat and Sentinel-2 image archive. Open-source tools such as the desktop-based python toolkit *CoastSat* (Vos et al., 2019b) and web-based *CASSIE* (Almeida et al., 2021) have subsequently been developed to automate the task of shoreline extraction for a selected coastal location using information from the images stored in the short-wave infrared (SWIR) and red, blue, green (RGB) colour bands. Validation of these SDS tools indicate shoreline accuracy in the range of 10-15 m, which, through subpixel image processing techniques, is typically smaller than the pixel resolution of Landsat/Sentinel-2 imagery (10-30 m). Because of their multi-decadal length and approximately bi-weekly sampling frequency, these tools are well

suited to monitoring intra-annual to decadal shoreline variability (Hagenaars et al., 2018; Vos et al., 2019a).

In comparison to publicly-available satellite data, applications using commercial satellites have to date been relatively limited. This has been primary due to the inhibitive data cost of commercial satellite imagery, but also a result of their patchy data coverage (since data collection is primarily tasked to monitor certain locations) and their much shorter archive length compared to the multi-decadal Landsat and Sentinel-2 archive (Belward and Skøien, 2015). Nevertheless examples of commercial satellite imagery applied to the coast include ASTER (Dewi, 2019), QuickBird (Almonacid-Caballer et al., 2016), SPOT (García-Rubio et al., 2015), RapidEye (Duarte et al., 2018), IKONOS, WorldView-2 and GeoEye-1 (Ford, 2013). One emerging field of coastal monitoring using satellites is that of constellations comprising hundreds of small (10x10x30cm) cubesat micro-satellites equipped with RGB and infrared sensors. Of this range of micro-satellites, the constellation known as PlanetScope has been an industry leader. First launched in March 2016, the PlanetScope constellation comprises 130+ satellites (known as 'Doves') arranged in a sun-synchronous orbit around the earth with a swath size of 24 to 32.5km (Planet, 2020). Due to their small size, cubesat satellites are cheap to manufacture and launch relative to traditional custom-built satellites. Consequently, the PlanetScope fleet is regularly updated via opportunistic third-party rocket launches with improved satellite components and sensor upgrades. This also results in a temporal variability of available images at specific study sites of interest as more satellites come online and others are discontinued. The images used in this study contain three generations of sensors (PS2, PS2.SD, and PSB.SD). The reader is referred to the Planet documentations for full details and additional sensor upgrades (Planet, 2020). A summary of PlanetScope history and imaging capabilities relative to Landsat and Sentinel-2 missions is presented in Figure 1.

Compared to the monthly to bi-weekly temporal resolution of Landsat and Sentinel-2 images, the PlanetScope Dove constellation is capable of sampling at daily to sub-daily resolution (Figure 1b). Additionally, the pixel size of PlanetScope is 3.7m at nadir (resampled to a 3 m fixed resolution), which is significantly greater than the 10-30 m resolution of Landsat and Sentinel-2 imagery (Figure 1c). However, the current generation of PlanetScope images do not contain the SWIR band that is commonly used in mapping satellite-derived shorelines. As such, the tools developed for Landsat and Sentinel images cannot be directly applied to this new and high-resolution data source. If other image bands (such as RGB, and near-infrared)

can be shown to accurately capture the shoreline position, this opens up the opportunity for much higher resolution shoreline analysis (Kelly and Gontz, 2019). With a growing image archive, the high spatial resolution and frequent revisit period of PlanetScope imagery has the potential to provide both long-term and discrete storm event monitoring at a consistent temporal resolution that has previously been unattainable outside of fixed remote sensing

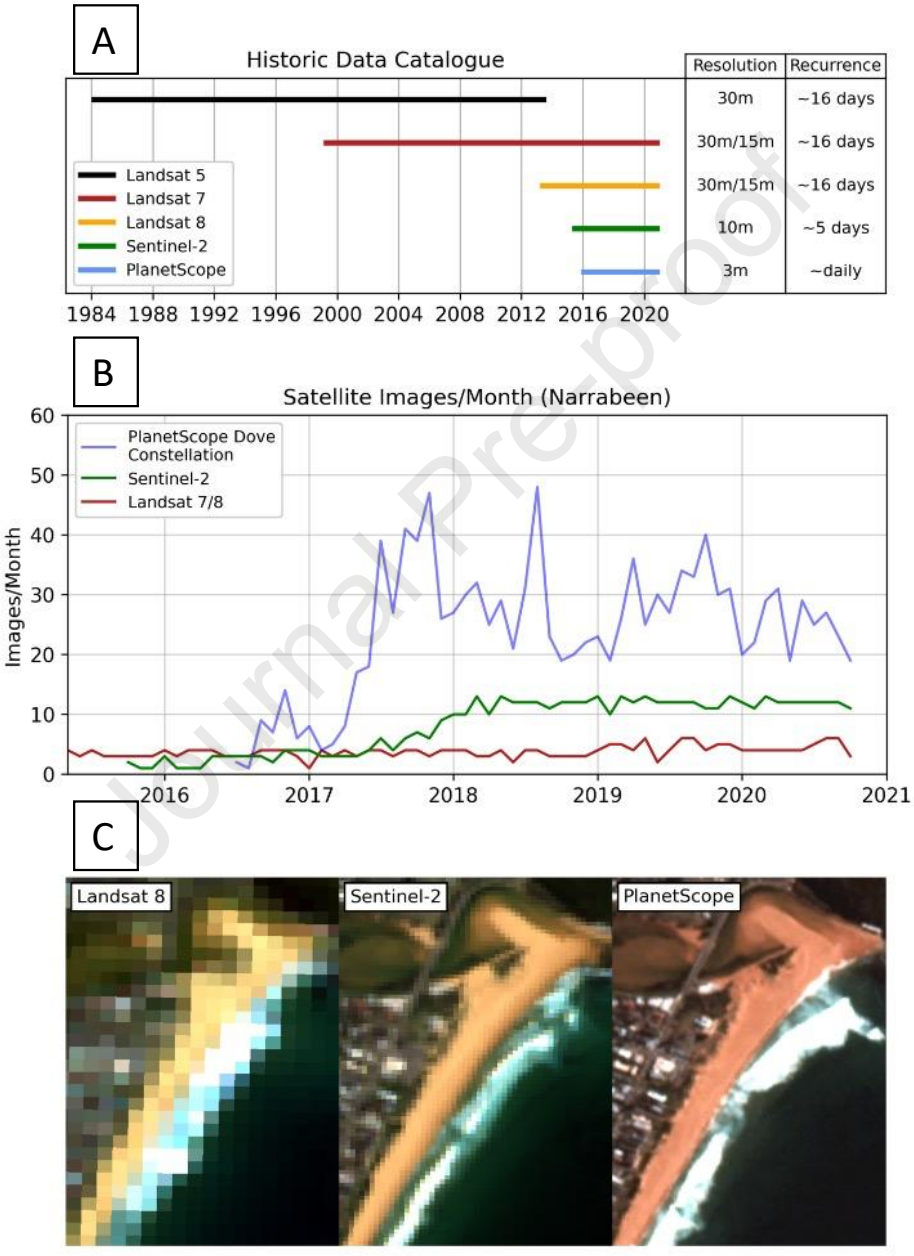


*Figure 1 – Comparison between Landsat 8, Sentinel-2 and PlanetScope Dove satellite missions. A) data catalogue. B) images per month collected at Narrabeen-Collaroy (2016-2020), and C) example raw images highlighting image resolution from the three sensors. Note that Landsat 7 & 8 have a higher resolution panchromatic band allowing for image pan-sharpening to a resolution of 15m that is not included here.*

shoreline monitoring stations, such as video camera networks (Bracs et al., 2016; Harley et al., 2019; Holman and Stanley, 2007). Notably, this technology has the potential to do so for any coastline on earth, every day. However, more information is needed into the best methodology to extract shoreline features from these images.

This paper presents a new open-source toolkit, *CoastSat.PlanetScope* that builds on the popular *CoastSat* package of Vos et al. (2019b) and is described in Section 2. The *CoastSat* package was originally developed and optimized for Landsat and Sentinel-2 imagery (using the Google Earth Engine API) and has since been applied at many locations worldwide, including Europe (Castelle et al., 2021), Australia (Cuttler et al., 2020), Africa (Lawson et al., 2021) and Asia (Adebisi et al., 2021). However, the application of satellite shoreline detection to PlanetScope imagery requires adaptation of the original *CoastSat* algorithm to address some new data challenges, as well as potential improvements associated with the increased accuracy and frequency of the PlanetScope products. First, the reduced number of spectral bands provided by PlanetScope cubesats (specifically the lack of a short-wave infrared band) means that the Modified Normalized Difference Water Index (MNDWI, refer Xu, 2006) that underpins *CoastSat* cannot be utilized for shoreline detection. As such, this work focuses on optimizing a new shoreline extraction algorithm based on the available PlanetScope bands of Red, Green, Blue, and Near-Infrared. Second, as the spatial resolution of the PlanetScope imagery is significantly higher than that of LandSat and Sentinel-2, the potential improvement in shoreline accuracy when correcting for both tides and waves (as opposed to just tides in the original *CoastSat* algorithm) is also explored.

Application of this new *CoastSat.PlanetScope* toolbox is validated at Narrabeen-Collaroy Beach in south-east Australia. With a high-quality multidecadal shoreline monitoring program well established at the site (Turner et al., 2016b), the Narrabeen-Collaroy dataset includes monthly surveys along five cross-shore transects, with additional surveys performed before and after major erosive events. A storm erosion case study investigates the ability of PlanetScope derived shorelines to monitor alongshore variable erosion during discrete storm events. Lastly, a blind validation of the toolkit is performed at Duck, North Carolina, USA using a generalized water level correction method.

## 2. Toolkit overview and testing

The overall workflow for the *CoastSat.PlanetScope* toolkit is outlined in Figure 2 and comprises several key steps from raw image data to shoreline products: 1) PlanetScope image pre-processing; 2) image band extraction and thresholding; and 3) shoreline extraction and elevation correction.

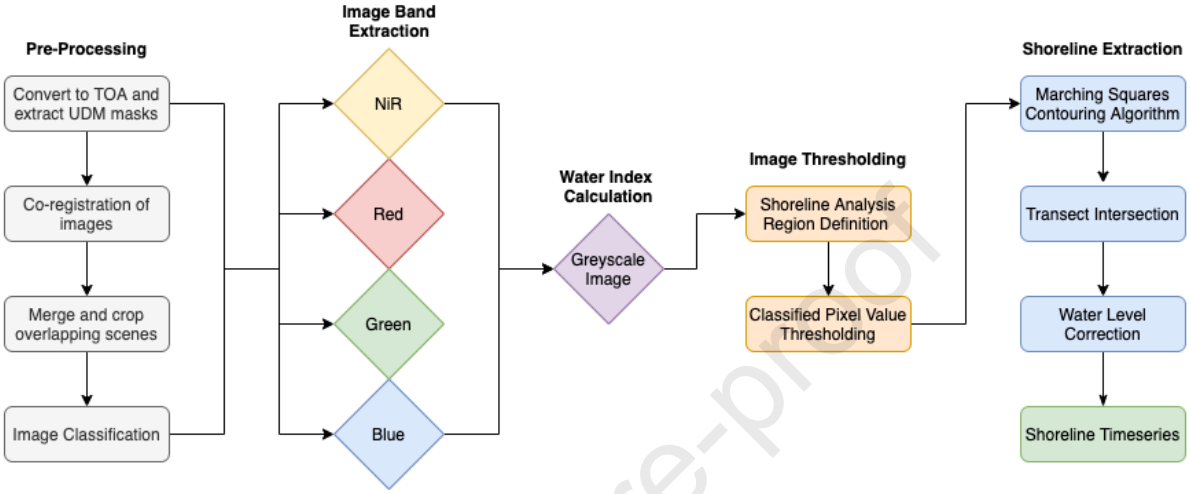


*Figure 2 – Shoreline extraction algorithm workflow for CoastSat.PlanetScope.*

Briefly, once the user has defined an area of interest, in Step 1, raw Digital Number PlanetScope images (RBG, NIR) are pre-processed to Top of Atmosphere (TOA), cropped and merged to the area of interest, co-registered and classified with a pre-trained supervised machine learning neural network algorithm. In Step 2, the 4 bands (RGB, NIR) are used to calculate a water index (e.g., NDWI, Red minus Blue) and a greyscale image from which the shoreline is extracted with the Marching Squares contouring technique based on an image-specific threshold. Finally, the 2D shorelines are intersected with shore-normal transects and the water level correction is applied along each transect. A more detailed description of the workflow is provided in Sections 2.2 and 2.3 below.

Algorithm testing and optimization were undertaken using *in situ* shoreline measurements from the Narrabeen-Collaroy coastal monitoring site (hereafter "Narrabeen"), a dynamic sandy beach located in south-east Australia where continuous beach measurements have been undertaken since 1976 (Turner et al., 2016b). A total of 24 combinations of indices, thresholding methods and elevation models are tested to obtain an optimal combination that is subsequently adopted in the toolkit. The application of the toolkit at Narrabeen provides a useful demonstration for the user and a step-by-step workthrough is provided in an accompanying Jupyter notebook.

## *2.1. Narrabeen testing site*

Narrabeen is located on the Northern Beaches of Sydney, Australia (refer Figure 3) and is one of the longest continuously monitored beaches worldwide (Turner et al., 2016b). Its open-access dataset is used as a testbed for a range of coastal remote sensing applications, including shorelines derived from Landsat/Sentinel-2 (Liu et al., 2017; Luijendijk et al., 2018; Vos et al., 2019a), coastal imaging (Harley et al., 2011) and smartphones (Harley et al., 2019). At approximately 3.6 km in length, the Narrabeen embayment is bounded to the north by Narrabeen Head and to the south by Long Reef Point. Narrabeen exhibits a microtidal tide regime with a mean spring range of 1.3 m. The deep-water wave climate is primarily composed of SSE swell waves with a mean significant wave height ($H_s$) of 1.6 m, a mean peak wave period ($T_p$) of 10 s and a storm wave height defined by $H_s$ > 3m (corresponding to the 5% exceedance of $H_s$). Nearshore wave conditions vary significantly alongshore due to sheltering from Long Reef Point of the predominantly southerly waves, with the northern end characteristically more exposed to the persistent southerly waves and southern end relatively sheltered (Turner et al., 2016b). The beach is primarily composed of fine to medium-grained quartz sand with a $D_{50}$ of approximately 0.3 mm. The intertidal beach slope varies significantly through time, with typical variability between 0.07 – 0.13 and an average intertidal slope of 0.09 (Vos et al., 2020a). The shoreline varies at weekly to monthly timescales due to the frequent passing of storms and subsequent beach recovery (Phillips et al., 2017). In addition, annual and interannual variability (on the order of 50m) is also visible over the 40 years of monitoring (Turner et al., 2016b).

For the purpose of algorithm testing, *in situ* survey data at Narrabeen were utilized for the time period July 2016 (coinciding when PlanetScope imagery first became available at the site) to August 2020. These measurements comprise 90 individual *in situ* survey dates at an average interval of 16 days. *In situ* surveys were conducted using RTK-GNSS (vertical accuracy ≈ ± 0.05 m, horizontal accuracy ≈ ± 0.03 m) at the five historical cross-shore transects that have been measured continuously since 1976 (profiles PF1, PF2, PF4, PF6, and PF8, Figure 1). Following previous studies (e.g., Harley et al., 2011), cross-shore shoreline positions were defined at these transects using the intersection of the surveyed profile with Mean High Water Springs (MHWS), which corresponds at this site to an elevation of 0.7 m Above Mean Sea Level (AMSL). The MHWS elevation has been shown to be a suitable reference datum for mapping shoreline variability at this site as it minimizes the influence of ephemeral low-tide

features such as low tide terraces and swash bars on shoreline variability (Phillips et al., 2017). In addition to the routine surveying, high resolution (50-100 m transect spacing) survey data was also collected using RTK-GNSS for a significant storm event that occurred between 8-10 February, 2020. This storm was characterised by waves over 3 m ($H_s$) from an ESE direction for a duration of 39 hours, reaching a peak $H_s$ of 6.5 m on 9 February. High-resolution rapid-response survey data were collected both two days prior to the storm (6 February, 2020) and four days after storm conditions subsided (14 February, 2020). These additional high-resolution data enabled to evaluate the capacity of PlanetScope-derived shorelines to capture alongshore variability in erosion following a large storm.

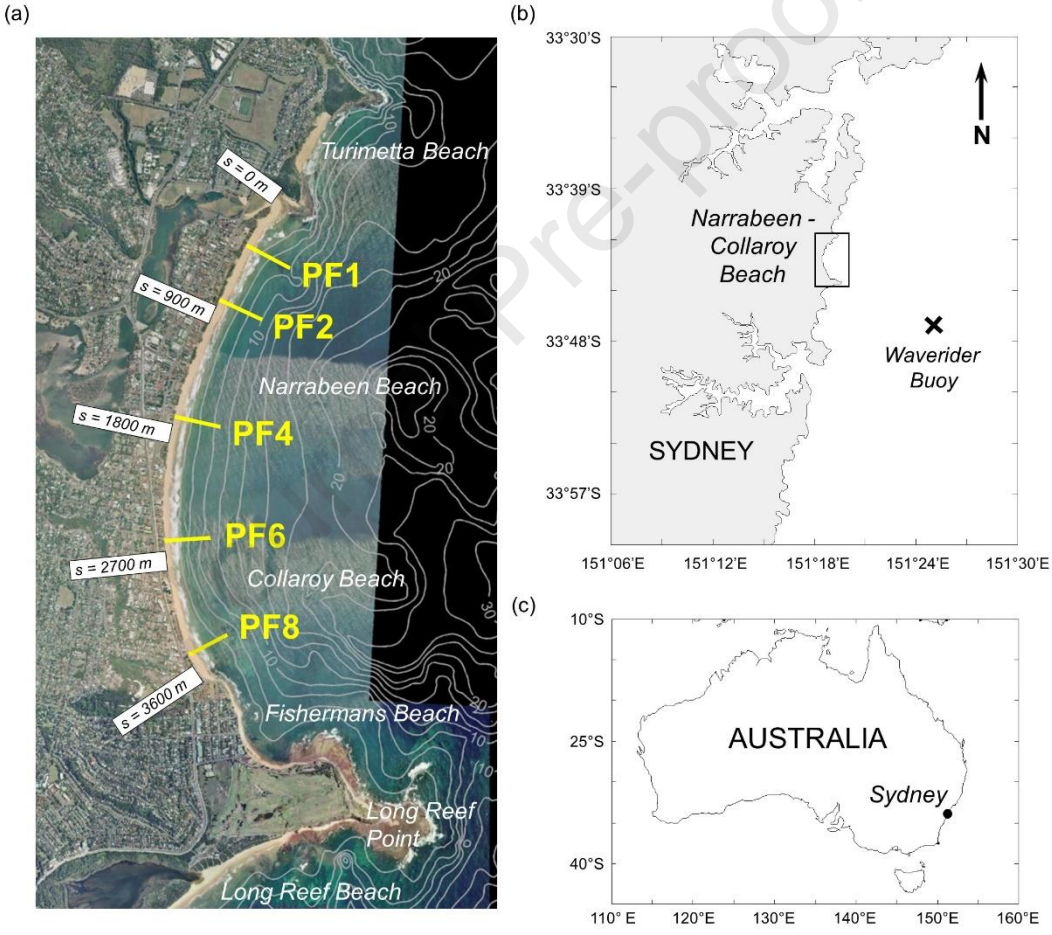


*Figure 3 – Narrabeen-Collaroy study site indicating locations of the five historical survey transects (PF1, PF2, PF4, PF6 and PF8).*

## *2.2. PlanetScope image pre-processing*

Imagery supplied by Planet from the PlanetScope satellite constellation is distributed into three data products, all based on raw sensor data captured at an average ground sample distance of

3.7 m at nadir (Planet, 2020). The four-band (Red, Blue, Green and Near Infra-Red) 'Analytic Ortho Scene' product is specifically used for shoreline mapping and tested in this study. This product orthorectifies and resamples image pixel data from a 3.7 m pixel resolution at nadir to a consistent 3 m pixel resolution, with data provided as Digital Number (DN) values that correspond to at-sensor detected radiance. To reduce scene-to-scene variability and enable direct comparison between images (Chander et al., 2009), DN values were converted in this study to Top of Atmosphere (TOA) reflectance via PlanetScope-provided conversion factors. An accompanying Unusable Data Mask (UDM) file is also provided for each image, to aid in the detection (and filtering) of sensor errors, data loss and regions of cloud cover.

The orthorectification accuracy of raw PlanetScope Analytic Ortho Scenes is stated at less than 10 m (Planet, 2020). Further independent studies have verified this accuracy, with observed horizontal RMSE values between 3.4 m and 5.2 m (Dobrinić et al., 2018; Lemajic et al., 2017). To reduce geolocation error prior to shoreline mapping, all individual downloaded images are co-registered. An image co-registration step is performed in the toolkit, using the open-source AROSICS library (Scheffler et al., 2017). Briefly, this co-registration software uses phase correlation in the frequency domain to automatically detect and correct sub-pixel misalignments between a reference image and a set of target images (RMSE of ~0.3 pixels). The reference image is chosen by the user from the available images where the image is focussed, cloud free and a shoreline can be seen clearly. Following this co-registration step, overlapping scenes from the same sensor on the same day are snapshots from a flyover and are merged and treated as one scene. To reduce unnecessary data, and processing times, an area of interest (AOI) is subsequently defined by the user to crop the images. After merging and cropping images, image pixels in the Ortho Scene then undergo an image classification where one of four separate classes are identified: *sand*, *water*, *whitewater* and *other* (where other refers to various features such as buildings, roads, vegetation, etc.). This image classification is undertaken using a Neural Network Multilayer Perceptron in the open-source Python toolkit *scikit-learn* (Pedregosa et al., 2011) in line with the methodology presented in *CoastSat* (Vos et al., 2019b).

A total of 572 PlanetScope Analytic Ortho Scenes at Narrabeen (spanning 457 unique dates) were downloaded for the July 2016 to August 2020 testing period. These 572 images were selected based on a cloud cover threshold (over the entire scene) of 50% or less, which from preliminary testing was found to remove the majority of unusable cloud impacted scenes at the

site. As the PlanetScope constellation has a sun-synchronous orbit, the vast majority of images occurred within an hour of the median local solar image timestamp at Narrabeen (~9:30 am). Due to the small fleet size in 2016, it was noted that image recurrence intervals were considerably more sporadic at the start of the study period, with a maximum time interval of 111 days recorded. As shown in Figure 1a, image recurrence increased significantly to near-daily from mid-2017 onwards with the launch of additional Dove satellite fleets. Training data for the image classification neural network was based on a subset of 25 images. These were manually digitized to include approximately 25,000 pixels for each of the image classes, except the *whitewater* class which only had 500 pixels. The classification accuracy was assessed by means of a 10-fold cross-validation which determined a pixel classification accuracy of 99.5%.

### *2.2.1. Shoreline Detection Algorithm*

With each scene corrected to the top-of-atmosphere, masked, co-registered, and classified, a generalized shoreline detection algorithm is then used to identify the two-dimensional shoreline position. This shoreline detection algorithm first creates a greyscale image based on a certain index (tested below), with a particular focus on the *water* and *sand* classes identified from the image classification step above. Next, a thresholding technique is applied to find the pixel value that delineates between water and sand pixels. Finally, a sub-pixel marching squares contouring algorithm (Cipolletti et al., 2012) is applied based on the identified threshold to identify the two-dimensional shoreline.

A total of six different spectral indices were tested at Narrabeen using combinations of the four bands available in the PlanetScope Analytic Ortho Scene. These indices were based on both absolute and normalised values of common water indices used in remote sensing applications (e.g., the Normalised Difference Water Index, McFeeters, 1996) as well as indices found suitable specifically for shoreline mapping based on colour bands only (e.g., Red minus Blue, Harley et al., 2019) . These six indices are defined below:

$$RmB = Red - Blue \quad (1)$$

$$RmB\ Norm = \frac{Red-Blue}{Red+Blue} \quad (2)$$

$$NmG = NiR - Green \quad (3)$$

$$NDWI = \frac{NiR-Green}{NiR+Green} \quad (4)$$

$$NmB = NiR - Blue \quad (5)$$

$$NmB\ Norm = \frac{NiR-Blue}{NiR+Blue} \quad (6)$$

where Red, Blue, Green and NiR correspond to the TOA values of each spectral band.

For each of these indices, two localized thresholding algorithms were investigated to determine the optimum threshold ($Index_{opt}$) for shoreline detection between sand and water pixels (as classified by the Neural Network described above). The two algorithms tested were the commonly-used Otsu thresholding technique (Otsu, 1976), as well as an alternate "Weighted Peaks" (WP) thresholding approach. The latter approach was developed by Harley et al. (2019) and calculated based on the location of the peaks in the probability density function (PDF) of the sand and water pixel index values. In contrast to the common Otsu thresholding (which maximises interclass variance), the WP thresholding algorithm weights the optimised index threshold towards the sand peak, which has been previously found to be robust for shoreline mapping purposes at a range of coastal locations worldwide (Plant et al., 2007, Harley et al., 2019). The optimum index based on WP thresholding is calculated as follows:

$$Index_{Opt,WP} = \hat{x}_{water} + 0.7(\hat{x}_{sand} - \hat{x}_{water}) \quad (1)$$

where $\hat{x}_{water}$ and $\hat{x}_{sand}$ are the x-location of the peaks in the PDF of the water and sand pixels, respectively. Following identification of the optimum threshold, the shoreline is identified along pixels of this optimum index value by means of a marching squares contouring algorithm (Cipolletti et al., 2012) that determines a 2D contour line via linear interpolation of adjacent cells values. An example of the entire shoreline detection process, from image classification, indexing, and thresholding for the specific case of the NmB index with WP thresholding is shown in Figure 4.

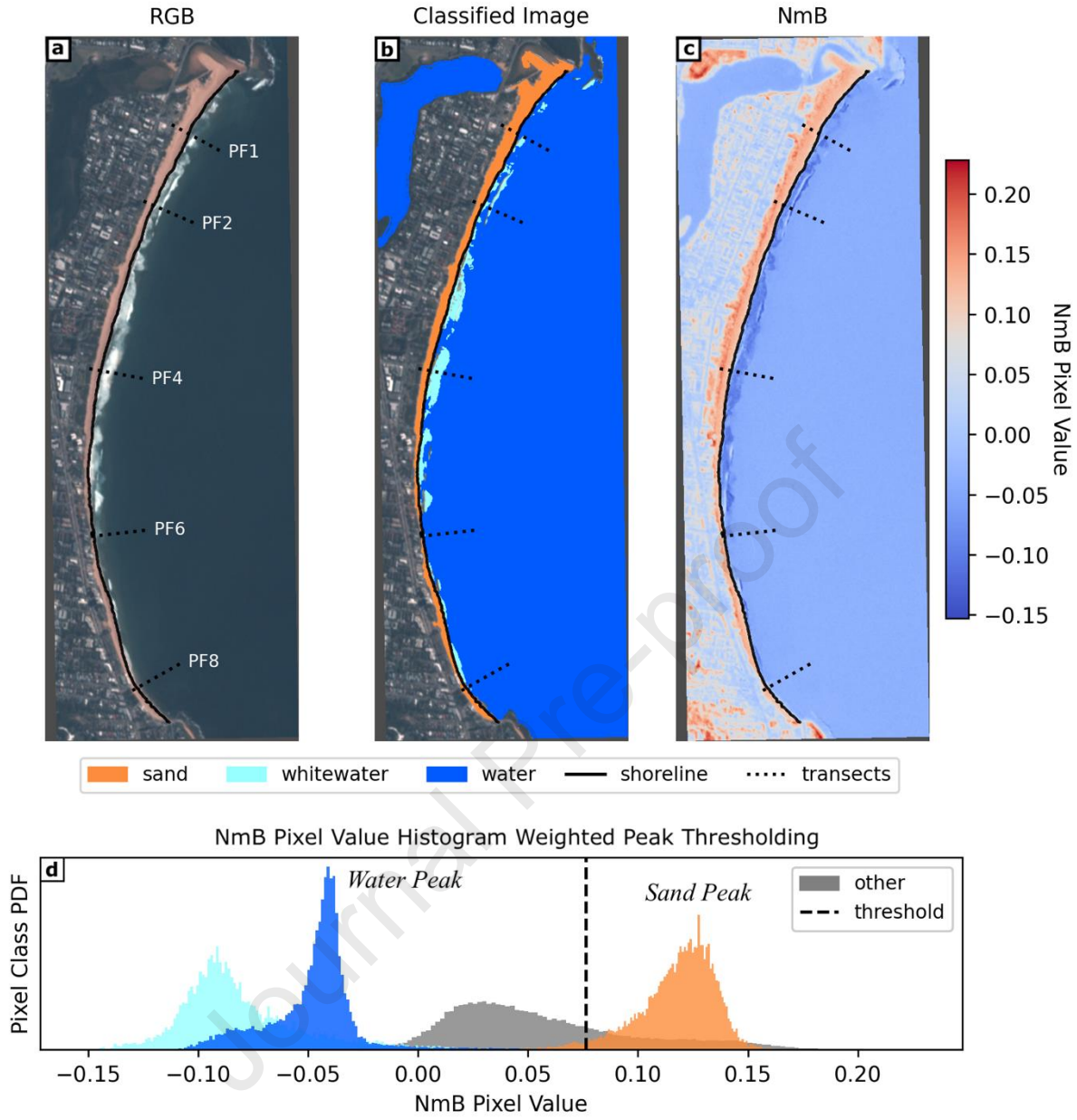


*Figure 4– Shoreline detection process from a PlanetScope Analytic Ortho Scene.* ***a)*** *PlanetScope satellite image superimposed with extracted shoreline and transect locations* ***b)*** *Neural-network classified output image highlighting sand, whitewater and water pixels* ***c)*** *Colourized greyscale NmB water index image* ***d)*** *Probability density function histogram of water index pixel values for each class and shoreline threshold value.*

## *2.3. Elevation correction model*

The following section outlines more advanced techniques that can be applied to further correct the extracted satellite-derived shoreline time series described above if the user desires. These techniques require various additional data sources that may include a time series of ocean water level elevations, intertidal beach slopes and wave characteristics. Astronomical tides (or observed ocean water levels) may be extracted from various sources at the user's discretion.

The intertidal beach slope may be derived from *in situ* data (e.g., beach profiles) or from remote sensing algorithms such as *CoastSat.slope* (Vos et al., 2020). Local wave time series (wave height, period) may be provided from local *in situ* wave buoys or from wave hindcasts/reanalysis.

Since satellite imagery represent an instantaneous snapshot of the coast, repeat shoreline measurements inherently include high-frequency (i.e., sub-daily) oscillations associated with rising/falling ocean water levels (tides + non-tidal anomalies), swash motions (wave setup and runup) as well as other factors (changing lighting conditions, beach morphology, granulometry, etc.). Previous approaches to reduce this inherent noise have been to either map satellite-derived shorelines on composite images averaged over large (i.e., annual) time windows (Almeida et al., 2021; Bishop-Taylor et al., 2021; Liu et al., 2017; Luijendijk et al., 2018), or apply an elevation correction model to correct for/reduce these high-frequency effects (Castelle et al., 2021; Pardo-Pascual et al., 2018; Vos et al., 2019a)

Based on lower-resolution (>10 m) Landsat and Sentinel-2 images, a simple tidal correction ($\Delta x_{tide}$) has been previously applied to project the cross-shore shoreline position detected by the satellite ($x_{sat}$) to a consistent elevation based on a specific elevation datum ($x_{DATUM}$):

$$x_{DATUM}(t) = x_{sat}(t) + \Delta x_{corr}(t) \quad (8)$$

$$\Delta x_{corr}(t) = \frac{z_{tide}(t) - z_{DATUM}}{m} \quad (9) \quad \text{(Simple tidal correction model)}$$

where $z_{tide}(t)$ is the ocean water level elevation at the time of image capture (taken from a nearby tide gauge), $z_{DATUM}$ is the reference elevation datum to define the shoreline and *m* is the intertidal beach slope.

Recognizing the potential for improved shoreline accuracy from high-resolution PlanetScope imagery, a more advanced elevation correction model was explored in this study where tide (or ocean water levels, intertidal beach slope and local wave conditions were known. As shown in Figure 5, the horizontal difference ($\Delta x_{corr}$) between the detected shoreline position $x_{sat}$ (measured in reference to the landward benchmark) and the datum-based shoreline can be

expressed as the linear sum of tidal effects ($\Delta x_{tide}$), wave effects ($\Delta x_{wave}$) and systematic biases due to the satellite detection method as well as any other remaining factors ($\Delta x_{det}$):

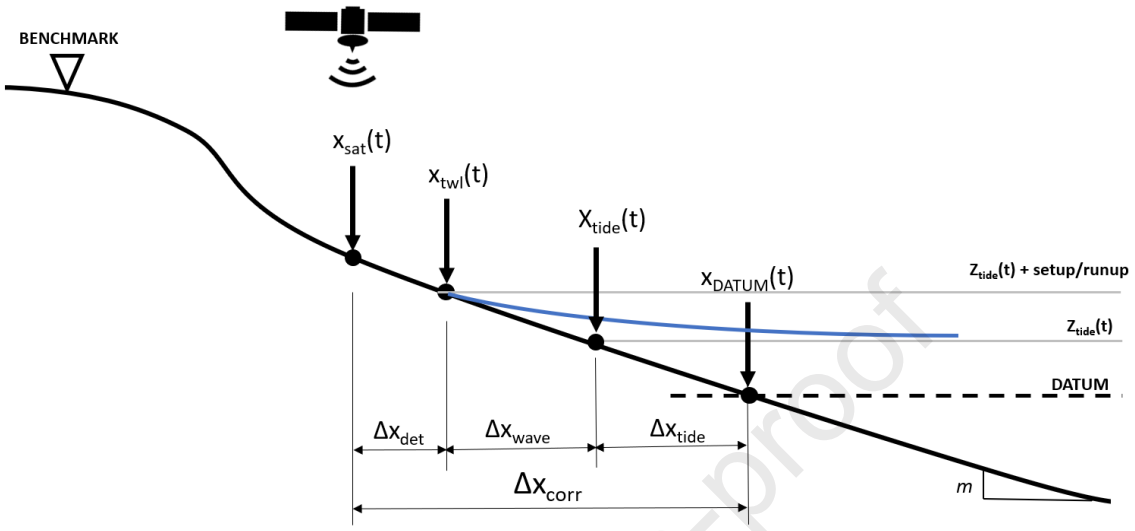


*Figure 5 – Schematic of elevation correction model to translate the instantaneous shoreline position derived from the satellite ($x_{sat}$) to a consistent elevation datum ($x_{DATUM}$).*

$$\Delta x_{corr}(t) = \Delta x_{tide}(t) + \Delta x_{wave}(t) + \Delta x_{det}(t) \qquad (10)$$

Following Eq. 3 in Harley et al., (2011), this is expressed by the empirical elevation correction model:

$$\Delta x_{corr}(t) = \alpha \frac{z_{tide}(t) - z_{DATUM}}{m} + \beta\sqrt{H_0(t)L_0(t)} + C \qquad (11)$$

where $\alpha$, $\beta$ and $C$ are empirically-derived parameters obtained from multiple linear regression (see below), $H_0$ is the deep-water significant wave height and $L_0$ the deep-water wavelength derived from linear wave theory. Note that where the coefficient of the simple tidal correction model (Eq. 9) used in previous studies is assumed to be equal to unity (i.e. $\alpha = 1$, representing the simple case of a planar beach face and no tidal modulations of other processes), here this coefficient is allowed to vary to potentially take into account other tidal effects. Time-varying wave runup/setup processes are incorporated in this elevation model via the second term in Eq. 11, which is derived from numerous lab and field observations (Holman, 1986; Hunt, 1959; Stockdon et al., 2006) that show that these processes scale well by $\sqrt{H_0 L_0}$. Similar to $\alpha$, here

$\beta$ is allowed to freely vary and does not take on any predefined value (e.g., 0.35 for Stockdon et al., 2006). The third term, *C*, represents any remaining systematic offsets (positive C corresponding to a landward bias), which is shown later can also include time-averaged wave runup/setup processes that are not accounted for in the second term.

The three parameters in Eq. 11 were solved at each of the five transects at Narrabeen using a least-squares multiple linear regression, based on the horizontal difference between the detected shoreline position $x_{sat}$ and the measured shoreline position at the reference datum (in this case, the 0.7m elevation corresponding to MHWS) obtained from RTK-GNSS surveys. Deep-water wave data were obtained from the Sydney waverider buoy, located 11 km offshore in 80 m water depth and ocean water-level data obtained from a nearby tide gauge (HMAS Penguin). Intertidal beach slopes *m* were calculated based on average values for each transect, derived from the RTK-GNSS surveys over the 2016-2020 study period. These equated to *m* = 0.11 (PF1, PF2, PF4), *m* = 0.13 (PF6) and *m* = 0.12 (PF8). While a time-invariant beach slope was chosen in this example, as in most cases worldwide where beach slope is not well resolved, it is acknowledged that a user may also wish to use a time-varying slope term if the data is available.

Finally, to test whether incorporating time-varying wave data improves the accuracy of PlanetScope shorelines at the validation site, an elevation model that removed the second term in Eq. 11 was also tested:

$$\Delta x_{corr}(t) = \alpha \frac{z_{tide}(t) - z_{DATUM}}{m} + C \qquad (12)$$

The two parameters of this model ($\alpha$ and *C*) were calculated using the same multiple linear regression process above.

# 3. Testing results

## 3.1. Optimal shoreline extraction methodology

To determine the optimal shoreline extraction methodology for the Narrabeen validation site, PlanetScope-derived shoreline positions were calculated at each of the five transects and compared with *in situ* data for all proposed extraction methodologies described above. Taking into account the six different indices tested (refer Eqs. 1-6), two thresholding algorithms (Otsu

and Weighted Peaks thresholding), and two elevation detection models (refer Eqs. 11-12), this amounted to 24 unique combinations. Shoreline results at all five transects were then combined to provide an overall summary of the residual error based on the cross-shore RMSE between PlanetScope-derived and measured shoreline positions at the reference datum (0.7 m AMSL).

Table 1 summarizes results for all 24 survey extraction methodologies. PlanetScope-derived shoreline accuracies were found to range from an RMSE of 3.5 m to 5.1 m. As discussed later in Section 4.3, this represents a substantial improvement in shoreline accuracy compared to equivalent efforts using Landsat and Sentinel-2 imagery at this site based on the *CoastSat* toolbox (RMSE = 8.2 m, Vos et al., 2019a). Four of these methodologies were found to have equally optimal accuracy, with each indicating a cross-shore RMSE between PlanetScope-derived and measured shoreline positions of 3.5 m. These four optimal methodologies were: using the Near-infrared minus Green (NmG, Eq. 3) or Near-infrared minus Blue (NmB, Eq. 6) indices; in combination with the Weighted Peak thresholding and either of the two elevation models (see Shoreline Extraction Method 6, 8, 14 and 16 in Table 1). The lowest-performing methodologies in terms of RMSE meanwhile were the normalized Red minus Blue (RmB Norm) index (Eq. 2) in combination with Otsu Thresholding and either of the two elevation correction models (see Shoreline Extraction Method 21 and 23, Table 1).

Comparing the results for each of the shoreline extraction methods, the analyses indicate a moderate sensitivity to the thresholding approach and index type, but a negligible sensitivity between the two elevation models tested (Eq. 11 vs Eq. 12). In terms of the thresholding approach, a 5-45% improvement in shoreline accuracy was found for each index when using the Weighted Peaks thresholding over the Otsu thresholding approach. The index meanwhile was particularly sensitive to whether normalizing was applied, with non-normalized indices (i.e., NmB, RmB and NmG) providing noticeably improved shoreline performance (average RMSE = 3.7 m) to those with normalizing applied (i.e., NDWI, NmB Norm and RmB Norm, average RMSE = 4.4 m). Regarding the elevation correction model, the addition of a time-varying wave runup and setup term to the shoreline elevation model (Eq. 11) only resulted in a <1% improvement in shoreline accuracy compared to the model with only ocean water level variability and a constant (Eq. 12). This suggests that at the steep beach morphology tested here, time-varying wave information, such as that sourced from a nearby wave gauge, might not necessarily be needed to improve shoreline accuracy (discussed in more detail in Section 4.1). Since four combinations were found to have equally optimal performance, only the

NmB/Weighted Peaks/Tide-only Model methodology (Method 8) was subsequently selected for further analysis below.

*Table 1. Summary of optimised elevation model parameters and shoreline accuracy for the 24 different extraction methodologies. The four optimal shoreline methodologies in terms of shoreline accuracy are highlighted in bold.*

| **Shoreline Extraction Method** | | | **Wave+Tide Model (Eq. 11)** | | | **Tide-only Model (Eq. 12)** | | **Shoreline accuracy (RMSE)** |
|---|---|---|---|---|---|---|---|---|
| | **Index** | **Thresholding** | **α** | **β** | ***C*** | **α** | ***C*** | |
| 1 | NDWI | Otsu | 0.97 | 0.01 | -3.8 m | - | - | 4.9 m |
| 2 | NDWI | WP | 0.97 | 0.07 | -0.3 m | - | - | 4.0 m |
| 3 | NDWI | Otsu | - | - | - | 0.76 | -3.6 m | 4.8 m |
| 4 | NDWI | WP | - | - | - | 0.96 | 0.7 m | 4.0 m |
| 5 | NmB | Otsu | 0.96 | 0.01 | 1.5 m | - | - | 3.7 m |
| **6** | **NmB** | **WP** | **0.95** | **0.01** | **5.0 m** | **-** | **-** | **3.5 m** |
| 7 | NmB | Otsu | | | | 0.96 | 1.6 m | 3.7 m |
| **8** | **NmB** | **WP** | | | | **0.95** | **5.2 m** | **3.5 m** |
| 9 | RmB | Otsu | 0.98 | 0.01 | 2.7 m | - | - | 3.9 m |
| 10 | RmB | WP | 0.90 | 0.02 | 5.0 m | | | 3.8 m |
| 11 | RmB | Otsu | - | - | - | 0.98 | 2.8 m | 3.9 m |
| 12 | RmB | WP | | | | 0.9 | 5.3 m | 3.8 m |
| 13 | NmG | Otsu | 0.90 | 0.02 | 0.8 m | - | - | 3.7 m |
| **14** | **NmG** | **WP** | **0.92** | **0.01** | **4.5 m** | | | **3.5 m** |
| 15 | NmG | Otsu | | | | 0.90 | 1.2 m | 3.7 |
| **16** | **NmG** | **WP** | | | | **0.92** | **4.8 m** | **3.5 m** |
| 17 | NmB Norm | Otsu | 1.07 | 0.01 | -3.0 m | - | - | 4.4 m |
| 18 | NmB Norm | WP | 1.03 | 0.05 | 0.7 m | - | - | 4.0 m |
| 19 | NmB Norm | Otsu | | | | 1.06 | -2.8 m | 4.4 m |
| 20 | NmB Norm | WP | | | | 1.03 | 1.4 m | 4.0 m |
| 21 | RmB Norm | Otsu | 1.03 | 0.04 | -2.5 m | - | - | 5.0 m |
| 22 | RmB Norm | WP | 0.97 | 0.06 | 0.5 m | - | - | 4.2 m |
| 23 | RmB Norm | Otsu | - | - | - | 1.04 | -1.8 m | 5.1 m |
| 24 | RmB Norm | WP | - | - | - | 0.97 | 1.3 m | 4.3 m |

Figure 6 presents the corresponding time series of shoreline change at each of the five transects in comparison to *in situ* measurements, using Method 8. Overall, there is a strong agreement between the *in situ* and PlaneScope-derived shorelines, with the PlanetScope-derived shorelines describing between 86% and 91% of shoreline variation over the four-year time period. This includes seasonal cycles of erosion and accretion, high frequency (i.e., monthly) shoreline variability as well as episodic storm erosion and recovery such as that observed in the February 2020 storm at the end of the time series (see Section 3.3 below). Note that profile PF6 is backed by a seawall (cross-shore location shown in Figure 6 by red-dash line) and shoreline points were subsequently truncated landward of this mark. On a transect-by-transect basis, the RMSE using this optimal methodology was found to vary from a minimum RMSE of 2.9 m (PF8) to a maximum RMSE of 4.2 m (PF1). These minimum and maximum errors coincide with the most sheltered and most exposed parts of the embayment in terms of wave energy, which suggests that error is enhanced by increased individual swash motions at the more exposed location (PF1) and reduced in regions of lower wave activity (PF8).

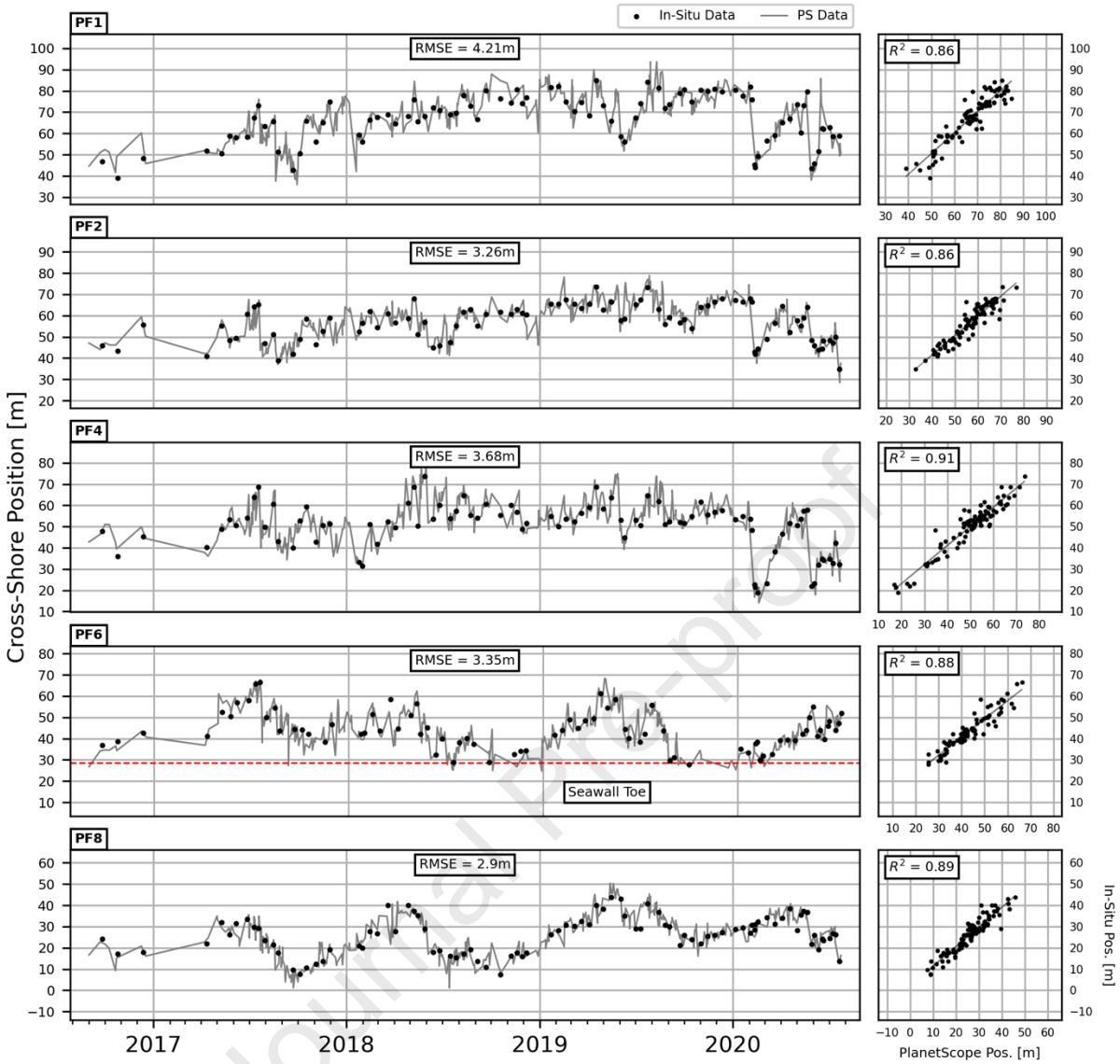


*Figure 6 – Time series of cross-shore shoreline change along five transects at Narrabeen-Collaroy derived from both PlanetScope imagery and in-situ topographic surveys.*

## *3.2. Elevation Correction Model Parameters*

The results above were based on optimized parameters of the two elevation correction models tested, using multiple linear regression of the shoreline data combined from all five beach transects. These parameters were the tidal correction model coefficient $\alpha$, the time-varying wave runup/setup coefficient $\beta$ and the constant $C$ accounting for any remaining systematic offsets, as summarized in Table 1. Across all 24 survey extraction methodologies, the tidal correction model coefficient was found to be close to unity ($\alpha$ = 0.9 to 1.07), suggesting that the simple planar profile is a suitable approximation for tidal corrections at this site. For the 12

methodologies that also included the additional time-varying wave runup/setup term, the coefficient β was found to vary from 0.01 (Methods 1, 5, 6, 9 and 14) to 0.07 (Method 2). The constant *C* meanwhile resulted in a wide range of optimized values, from negative values that represent a systematically more seawards horizontal offset (*C* = -3.8 m, Method 1) to positive values characterising a systematically more landwards offset (*C* = 5.3 m, Method 12). Generally, there was little variability in the constant *C* between the tide and wave model and the tide-only model for each index and thresholding (average difference between the two optimised C values = 0.3 m). For the selected Method 8, a tidal correction model coefficient of α = 0.95 and a constant horizontal offset *C* = 5.2 m was found.

### *3.3. Performance of PlanetScope-derived shorelines on individual extreme storm response*

In addition to evaluating the accuracy of PlanetScope imagery in obtaining time series of shoreline change (e.g., Figure 6), a key capability explored in this study was the ability of PlanetScope-derived shorelines to map alongshore variability in shoreline change following an extreme episodic storm event. Figure 6 presents comparisons between pre- and post-storm shoreline positions derived from both PlanetScope imagery (using the optimal shoreline extraction methodology identified above) and RTK-GNSS survey data, for the large storm event that struck the coastline at Narrabeen between 9-10 February, 2020. These comparisons were undertaken for both the individual pre- and post-storm shoreline positions (Figure 7a) as well as for the alongshore variability in shoreline change resulting from the storm (Figure 7b). PlanetScope imagery for shoreline mapping was selected five days prior to storm and just two days after the storm, based on the nearest available data spanning the storm event.

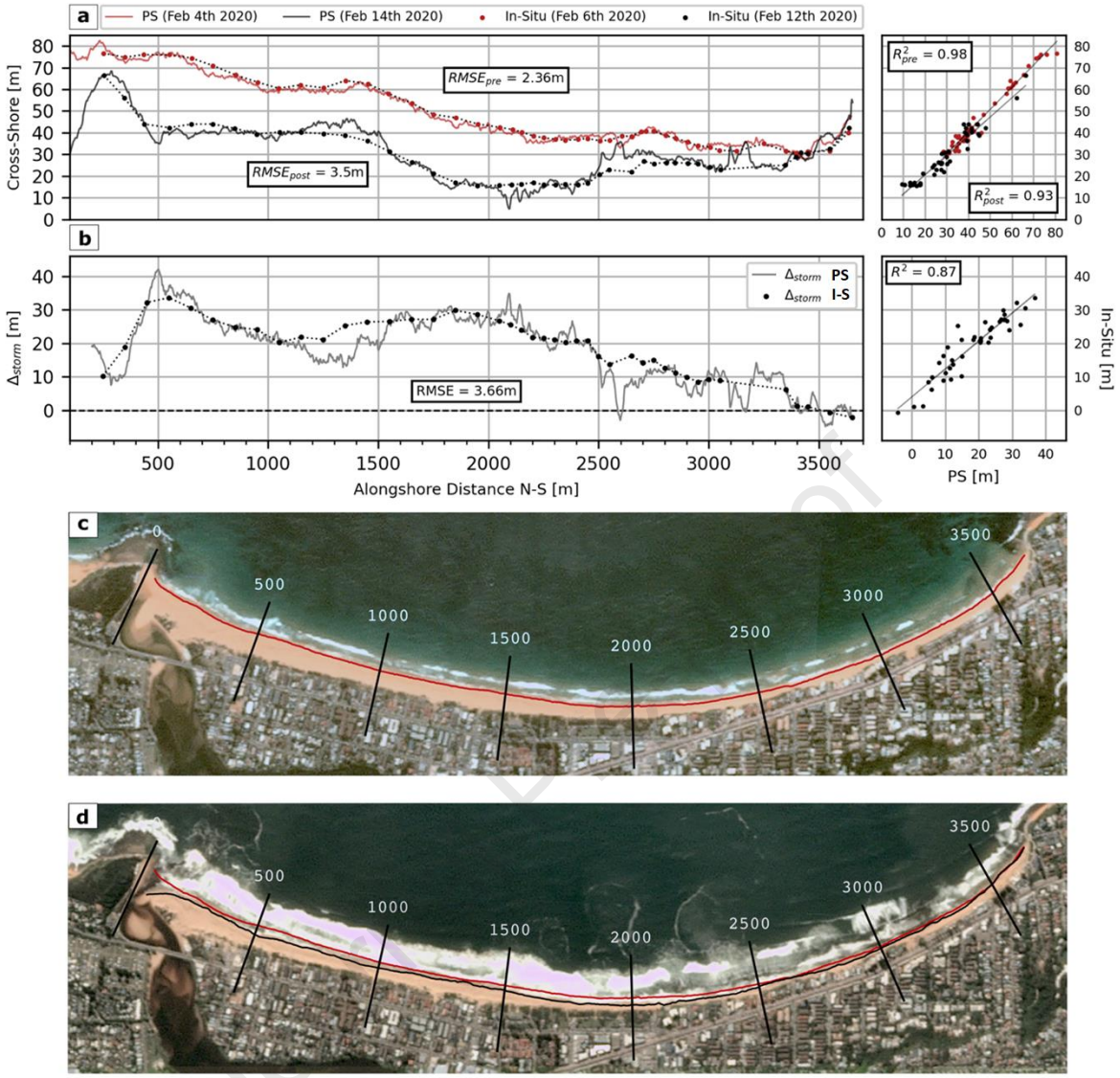


*Figure 7 – **a)** Comparison between pre- and post-storm alongshore PlanetScope (PS) shoreline position relative to in-situ (I-S) survey data measured using RTK-GNSS. **B)** Comparison between PlanetScope and in-situ cross-shore shoreline position change over the duration of the storm event. **c)** Pre-storm PlanetScope satellite image (February 4, 2020) overlayed with pre-storm PS shoreline. **d)** Post-storm PlanetScope satellite image (February 14, 2020) overlayed with pre-storm (red) and post-storm (black) shorelines.*

Overall, a strong agreement was found between individual pre- and post- storm shorelines ($R^2$ = 0.98 and 0.93, RMSE = 2.4 m and 3.5 m, respectively) derived from PlanetScope and *in situ* RTK-GNSS shoreline measurements at the reference datum. Examining the difference between pre- and post-storm shorelines, Figure 7b presents the change in shoreline due to the storm as determined by PlanetScope shorelines and *in situ* measurements, respectively. This figure indicates significant alongshore variability in storm erosion, with some 'hotspots' (local maxima) of shoreline erosion observed at 600 m alongshore (measured shoreline change = 34

m) and 1800 m alongshore (measured shoreline change = 30 m). A general trend of enhanced shoreline retreat at the northern end (<2000 m alongshore) compared to the southern end (>2000 m alongshore) is also evident in the RTK-GNSS measurements. The corresponding PlanetScope-derived shoreline change measurements also show good agreement with these general trends and local maxima, such that the overall RMSE is 3.66 m and $R^2$ = 0.86. The alongshore-averaged shoreline change for the entire 3.6 km beach was also estimated accurately by the PlanetScope data, with 18 m of shoreline change for the PlanetScope-derived shorelines and 19 m for the RTK-GNSS survey data.

# *4. Discussion*

## *4.1. Optimized elevation correction model parameters*

Optimization of the model parameters used to correct for elevation differences between the instantaneous PlanetScope-derived shorelines and the reference datum provide crucial insights into the shoreline detection performance. Regarding the tidal correction term, the model coefficient $\alpha$ was found to be roughly equal to the value of unity typically assigned for tidal correction, based on the assumption of a planar beach face and no tidal modulation of elevation differences (Castelle et al., 2021; Vos et al., 2019a; Zhang et al., 2021). This suggests that these assumptions are valid for the Narrabeen-Collaroy site, with small differences likely due to subtle beach slope ($m$) changes over time that are not accounted for in the satellite derived shoreline elevation correction model. Tidal correction based on a time-varying beach slope was also trialled, although this resulted in a reduction in shoreline accuracy relative to time-averaged values.

For the wave runup/setup term, comparisons between optimized models both including and excluding time-varying wave runup and setup found negligible differences in terms of PlanetScope-derived shoreline accuracy. This result suggests that time-varying wave setup and runup is not an important consideration in PlanetScope shoreline mapping at the Narrabeen site. The practical implication of this finding is that it suggests there might be little advantage in terms of shoreline accuracy in including time series of wave variability, which is often difficult to obtain without ready access to *in situ* wave measurements from a nearby wave buoy. It should be noted that this result is likely to be site-specific and related to the steep and microtidal nature of the Narrabeen site. For example, in southwest France, Castelle et al., (2021) found using lower resolution Landsat imagery that shoreline accuracy was improved by

a factor of two when a time-varying wave runup equation was included in the elevation correction model. This was attributed to the low beach face gradient ($m$ = 0.05) and energetic and highly seasonal wave conditions at this site (average Hs = 1.1 m / 2.4 m in summer/winter, respectively). Such conditions can result in much larger horizontal variations in wave runup relative to steeper beaches with less seasonally varying wave climates like Narrabeen. Further validation of this new algorithm across a range of sandy beach environments is needed to explore the robustness of this result.

The influences of wave runup and setup processes on the PlanetScope-derived shoreline position at Narrabeen instead appear to be captured within the constant offset term $C$. Figure 8 illustrates the alongshore variability in both $\alpha$ and $C$ for each transect along the beach using the Method 8 combination comprising the NmB Index, the Weighted Peaks thresholding and the tide-only elevation correction model. A distinct gradient in the offset term (Figure 8b) is indicated that appears similar in shape to the variability of wave exposure along the beach, with $C$ = 4.0 m at the most sheltered profile (PF8) and $C$ = 5.5 m to 6.2 m for the three northern profiles exposed to the predominantly SSE waves of the region (PF1, PF2 and PF4). To further explore alongshore variability in wave runup and setup effects, the optimised $C$ term at each transect was subsequently compared to that estimated from a standard wave setup equation at the shoreline (Stockdon et al., 2006, eq. 10). This is expressed horizontally as:

$$\frac{\langle \eta \rangle}{m} = 0.35\sqrt{H_0 L_0} \qquad (13)$$

where $\frac{\langle \eta \rangle}{m}$ is the estimated horizontal offset by wave setup at the shoreline. Using Equation 13, the average (time-invariant) horizontal offset by wave setup was estimated at each transect by first transforming average offshore wave conditions at Narrabeen ($H_0$ = 1.6 m, $T_p$ = 10 s, $\theta$ = 135°) to the 10 m depth contour, using a nearshore wave transformation tool based on 1000s' of SWAN model runs (refer to Turner et al., 2016b). Since Equation 13 is based on deep-water conditions, this wave data at the 10 m depth contour was then reverse-shoaled to give the equivalent deep-water wave conditions (i.e., $H_0$ and $L_0$) at each transect from which the wave setup was calculated. Estimates of $\langle \eta \rangle$ are shown as crosses in Figure 8b and reveal a reasonable agreement ($R^2$ = 0.60) between this offset term and that estimated using the wave setup formulation.

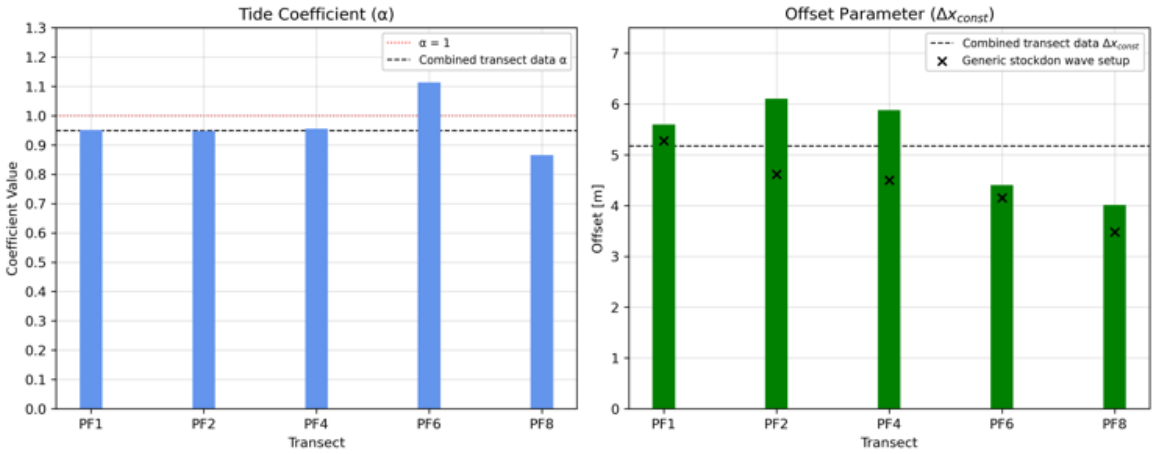


*Figure 8– Optimized coefficients of α (left panel) and C (right panel) in Equation 12 for each of the five transects at Narrabeen (PF1, PF2, PF4, PF6 and PF8). Crosses in the right panel denote estimates of time-averaged wave setup at the shoreline according to Stockdon et al., (2006).*

Deviations between the optimised *C* value and the estimated setup also only range from 0.1 m (PF6) to 1.5 m (PF2), suggesting that this systematic offset can be estimated using this commonly-used wave setup formulation.

## *4.2. Blind application of generalised elevation model at Duck, USA*

The above results are based on optimized model coefficients derived from extensive *in-situ* beach measurements, which are rare and only available at a small subset of sites worldwide (Turner et al., 2016a). To test the ability of *CoastSat.PlanetScope* to map shoreline variability at an unseen coastal location, the toolkit was applied blindly to PlanetScope imagery covering the U.S. Army Corps of Engineers Field Research Facility at Duck, North Carolina, USA (Zhang and Larson, 2021). The Duck Field Research Facility is an internationally-recognized coastal observatory located on the northern Outer Banks, a low-lying barrier island system. The beach slope at Duck is similar to that of Narrabeen ($m$ = 0.10) and has a similar microtidal and semidiurnal tide range (mean spring tidal range ≈ 1.1 m). Wave conditions are typically less energetic relative to Narrabeen (mean $H_s$ = 1.0 m, $T_p$ = 9 s) and interrupted by storm events (defined by a threshold $H_s$ > 2m) from hurricanes and Atlantic nor'easters. A 1.2 km stretch of coastline centred on a research pier has been monitored extensively at Duck since 1977, using a combination of survey techniques (O'Dea et al., 2019; Pianca et al., 2015). Here the blind application is focused on four cross-shore transects defined by the local alongshore reference

system oriented roughly from SSE to NNW: PF -91 m, PF 320 m, PF 731 m and PF 1097 m (refer Zhang and Larson, 2021, Figure 2).

A total of 166 PlanetScope images were sourced at the Duck site over the period November 2017 to August 2020, equivalent to an average interval of one image every 6 days. Following the results above, shoreline detection was undertaken using the Method 8 combination as above. Two alternate steps were subsequently taken in order to make this application at Duck truly blind and not rely on any *in situ* beach measurements. To estimate the beach slope *m* needed for the elevation correction model (Eq. 12), the method of Vos et al., (2020b) was applied to the PlanetScope-derived shorelines. This algorithm estimates the beach slope by iteratively searching the optimum *m* value that minimises short-term shoreline variability in the frequency band of tidal constituents identified in the shoreline time series. Validation of this technique (including at both the Duck and Narrabeen sites) has found that the beach slope can be estimated to within ± 0.01. The application of this step identified beach slopes of 0.08 – 0.11 for the four Duck profiles. The second step comprised the use of a generalized elevation correction model, rather than relying on site-specific optimized model coefficients as undertaken at Narrabeen. Based on the findings above that the time-varying wave runup and setup term may have little practical benefit at some sites and that the constant offset *C* can be approximated using the Stockdon et al., (2006) formulation, the following generalized model was adopted:

$$\Delta x_{corr}(t) = \frac{z_{tide}(t) - z_{DATUM}}{m} + 0.35\sqrt{H_0 L_0} \qquad (14)$$

Tide conditions at the time of image capture were taken from the nearby tide gauge at the Field Research Facility.

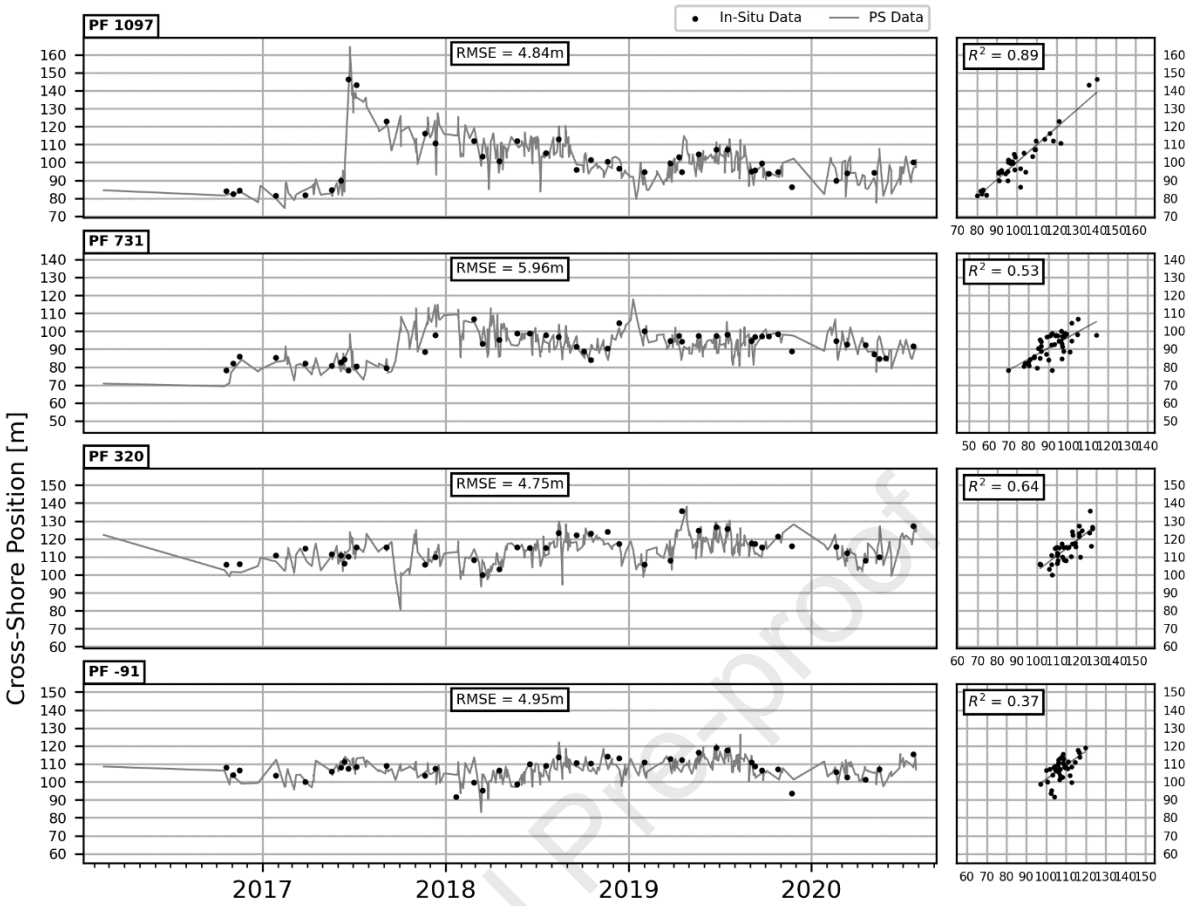


*Figure 9 – Blind application of the CoastSat.PlanetScope toolkit at Duck, North Carolina using a generalized elevation correction model. The effects of a sand nourishment project in mid-2017 are clear in profile PF1097.*

Figure 9 presents time series of PlanetScope-derived shorelines relative to *in situ* survey measurements at the four cross-shore profiles at Duck, using the same reference datum used at Narrabeen. Shoreline accuracy using this blind application is shown to vary from a minimum RMSE of 4.8 m (PF 320 m) to 6.0 m (PF 1097). This represents a slight decrease in shoreline accuracy relative to Narrabeen using site-specific optimized model coefficients, but is considerably more accurate when using lower resolution Landsat or Sentinel-2 imagery at Duck with the *CoastSat* algorithm (RMSE = 9.0, Vos et al., 2019a). The increase in accuracy obtained by PlanetScope imagery is subsequently sufficient to capture smaller-scale variability at the sub-annual or seasonal time-scales, particularly considering the generally smaller magnitude of shoreline variability at Duck relative to Narrabeen. This was identified as a key limitation of applying *CoastSat* and Landsat/Sentinel-2 at less dynamic sites (Vos et al., 2019a). Also evident in this time series is a significant artificial beach nourishment works that was undertaken at the northern end of the site (refer profile PF 1097, Figure 7) in May-June,

2017. The high-frequency imagery of the PlanetScope constellation meant that the shoreline both immediately before and immediately after the nourishment works could be mapped, enabling accurate quantification of the shoreline response to this engineering intervention. A corresponding 60 m increase in shoreline position is observed in this northern time series, which is followed by a gradual reduction as sediment is moved alongshore. Further south at profile PF 731, the shoreline is observed to increase approximately 30 m at a lag of approximately three months following the nourishment.

### *4.3. Benefits and challenges of PlanetScope imagery for shoreline mapping*

The Narrabeen beach monitoring site has been used as a testbed for a range of advanced coastal remote sensing applications (Splinter et al., 2018), thereby making it possible to compare the overall performance of PlanetScope-derived shoreline detection to other optical remote sensing applications. Table 2 summarizes results of previous shoreline accuracy tests applied at Narrabeen, including satellite-derived methods (Luijendijk et al., 2018; Vos et al., 2019a; this study), land-based video imaging using the Argus coastal imaging system (Harley et al., 2011) and a citizen science-based approach using consumer smartphones known as CoastSnap (Harley et al., 2019). These different approaches span a range of image pixel resolutions depending on the approach and sensor used, from 30 m for older Landsat-5 satellite missions (and no panchromatic-sharpening), to 0.1 m pixels for land-based Argus video imaging in the image nearfield. Note that whereas satellite imagery is typically close to nadir and hence have negligible resolution variability over the spatial scale of individual beaches (~kilometers), land-based approaches have significant variability in pixel resolution alongshore due to their low angle of obliquity (Holman and Stanley, 2007).

*Table 2. Comparison of different remote sensing methodologies applied at Narrabeen-Collaroy*

| **Methodology** | **Pixel Resolution** (*pan sharpened) | **Image Capture Type** | **Accuracy** | **Reference** |
|---|---|---|---|---|
| Landsat | 10-15 m* | Instantaneous | ~10 m | Liu et al. (2017) |
| Shoreline Monitor + Landsat/Sentinel-2 | 10-30 m | Annual composite | 13.7 m | Luijendijk *et al.* (2018) (Supplementary material Table X) |
| CoastSat + Landsat/Sentinel-2 | 10-15 m* | Instantaneous | 8.2 m | Vos et al., (2019a) |
| Digital Earth Australia Coastlines Landsat | 15-30 m | Annual median composite | 7.4 m | Bishop-Taylor et al. (2021) |
| *CoastSat.PlanetScope* | *3.7 m* | *Instantaneous* | *3.5 m* | *This study* |
| Citizen Science Smartphone (CoastSnap) | 0.2 m (nearfield) – 20 m (farfield) | Instantaneous (Time-averaged) | 1.4 m – 6.7 m (3.2 m) | Harley et al., (2019) |
| Argus Video Imaging | 0.1 m (nearfield) – 10 m (farfield) | Time-averaged | 1.2 m – 4.4 m | Harley et al., (2011) |

As expected, a general trend of increased shoreline accuracy with pixel resolution is observed in Table 2, with the PlanetScope-derived shorelines significantly more accurate than Landsat and Sentinel-2-derived approaches (horizontal accuracy 7.4 m – 13.7 m), but less accurate than land-based methods using stationary video cameras or smartphones (minimum horizontal accuracy = 1.2 m for Argus Video Imaging). This suggests that further improvements could be made in satellite-derived shoreline accuracy with the addition of other very high resolution (VHR) satellite missions, such as the Maxar Worldview-3 satellites launched in 2014 (pixel resolution = 0.31 m, Turner et al., 2021). However, as shown in this study, the shoreline accuracy reported here (~3.5 m) is larger than the pixel resolution (3.7 m), which contrasts with past work using coarser satellite imagery and sub-pixel techniques. This may suggest a limit in the pixel resolution substantially reducing the overall shoreline detection error, with the remaining error attributed to unresolved processes such as individual swash motions.

Additionally, an important consideration with regards to accessing this VHR image data (including PlanetScope) is that it is presently limited to either restricted research licenses, organisations/countries with data sharing agreements, or cost-prohibitive pay-per-image funding models. For instance, the PlanetScope imagery obtained in this study was made available through Planet's Education and Research program that provides a monthly download quota of 5,000 $km^2$ to university-affiliated students and researchers. For the 4 years of data used in this study, the study area required up to 2 images per scene to cover the extents of Narrabeen-Collaroy and resulted in roughly 1000 raw images being downloaded and was

covered within a monthly download limit. For longer timescales and larger study areas, as well as more frequent passes of the Planet constellation, longer download times may be needed to meet the quota restrictions. This provides a major barrier for uptake of PlanetScope and other VHR imagery for routine shoreline monitoring and makes publicly available imagery like Landsat and Sentinel-2 or land-based approaches still appealing.

Another challenge of satellite-derived shorelines approaches such as PlanetScope is their present reliance on instantaneous snapshots of the coast from single satellite passes. The instantaneous sampling of what is typically a highly dynamic and turbulent land-water interface (particularly on wave-dominated coastlines like Narrabeen) introduces error into the shoreline detection, as high frequency swash motions are difficult to resolve using simple elevation correction models such as that proposed in Eq. 11 and 12. These errors are typically reduced in land-based approaches using time-averaging, where video frames over a certain time period (nominally 10 minutes) are averaged to smooth out these high-frequency motions. For example, Harley et al., (2019) compared shorelines mapped by both instantaneous images and time-averaged images averaged over 10 minutes and observed an 18% improvement in shoreline accuracy. Although not explored in this study, the growing constellation of Dove cubesats can result in multiple satellite passes over a single day (Figure 1). This sub-daily shoreline data could potentially be exploited as a rudimentary means of smoothing shoreline oscillations and reduce shoreline noise.

Along with routine shoreline mapping over many years, the findings of this study highlight the benefit of PlanetScope imagery for rapid quantification of shoreline response due to extreme storm events. With an approximate median image recurrence of 2 days (Figure 1), PlanetScope imagery is able to capture (pending cloud coverage constraints) the shoreline position both immediately prior to and following an extreme storm event striking the coast. As shown in Figure 7 for a storm event that occurred in February 2020, PlanetScope-derived shorelines were able to quantify not only the average shoreline change caused by the event, but significant detail regarding the alongshore variability in erosion as well as localized erosion hotpots at the spatial scale of approximately 100 m. The capability of PlanetScope imagery for rapid shoreline assessment was also investigated by Kelly and Gontz (2020), who applied PlanetScope-derived shorelines to assess the impact of a severe tropical cyclone (Cyclone Oma) that struck eastern Australia in February 2019. Horizontal deviations between PlanetScope and measured shorelines in their study (obtained from a Lidar survey) were found

to range between 0 m and 22 m, with a mean offset (equivalent to the parameter *C* in the present study) of 9 m. While the horizontal RMSE was not reported in Kelly and Gontz (2020), the seemingly lower accuracy range compared to the present study is likely due to their study being based on a single validation survey and PlanetScope shorelines were manually digitised, rather than using the more robust method detailed here. As highlighted in Table 1, the results show that significant improvements in shoreline accuracy can be obtained using an optimized combination of shoreline index, thresholding approach and elevation correction model and that these factors should be considered for accurate shoreline mapping using PlanetScope imagery.

As is the case with other satellite remote sensing toolkits (e.g. *CoastSat*), site specific calibration of the classifier and additional techniques to improve mapping on more diverse coastlines, including macrotidal coasts, will likely lead to improved site-specific accuracy. We now welcome the broader coastal remote sensing community to continue to build upon this open-source software package presented here.

## *5. Conclusions*

This study has presented a new open-source tool known as *CoastSat.PlanetScope* that enables users to map shorelines from the growing catalogue of high-resolution PlanetScope cubesat image products that have been operational since 2016. Building on the popular *CoastSat* toolbox developed for Landsat and Sentinel-2 imagery (Vos et al., 2019), the study explored both the optimal shoreline extraction technique needed for these new high-resolution image products, as well as the potential improvement in shoreline accuracy that could be obtained when including a more advanced elevation correction model. Robust testing and optimization of this new toolkit was first undertaken at Narrabeen-Collaroy Beach in south-east Australia, followed by a blind application at Duck, North Carolina to test its more generic applicability.

The conclusions of this study can be summarized as follows:

- Horizontal shoreline accuracy of PlanetScope shoreline detection using this toolkit was found to vary depending on detection methodology, from a minimum (optimal) shoreline accuracy of 3.5 m (RMSE) to a lowest accuracy of 5.1 m. The optimal shoreline methodologies identified were using either the Near Infrared minus Green band (NmG) or Near Infrared minus Blue band (NmB) indexes for distinguishing the

land/water interface, in combination with the "Weighted Peaks" thresholding technique.

- The inclusion of time-varying wave information in the elevation correction model resulted in negligible difference in shoreline accuracy compared to the elevation correction model comprising only tide variability and a horizontal offset term. Hence PlanetScope shoreline detection appears insensitive to time-varying wave conditions at Narrabeen, a relatively steep, microtidal beach.
- Application of PlanetScope shoreline detection for an extreme storm event that struck the study site in February 2020 found that this new technique can capture alongshore variability in shoreline change ($R^2$ = 0.86), including the identification of localized erosion hotspots along a coastal stretch. This represents a marked improvement compared to lower-resolution Landsat and Sentinel-2 derived shoreline mapping of coastal storm response (Vos et al., 2019).
- Using a generic shoreline elevation model based on a standard wave setup formula, the blind application of PlanetScope shoreline mapping to a contrasting site in the USA (Duck, North Carolina) found a comparable level of shoreline accuracy (RMSE = 4.4 m). While this offers encouragement for the application of this technique at a range of sandy environments globally, care should be taken especially for more dissipative environments where wave runup effects in particular are more pronounced (e.g., Castelle et al., 2020)

Providing over four years of imagery and a near-daily imaging frequency, PlanetScope imagery opens up the possibility to extract shoreline data at sampling frequencies and accuracies previously unattainable from existing satellite-derived shoreline capabilities using Landsat and Sentinel-2. As an expanding fleet of satellites with continual data collection, the value of PlanetScope imagery is only expected to increase into the future as further data is collected. It is envisaged that this open-source toolkit will help facilitate use of this new dataset and provide a valuable resource to the coastal research community.

## *Acknowledgements*

The authors would like to thank Planet for enabling free access to the archive of PlanetScope imagery via a standard research license. The Narrabeen-Collaroy coastal monitoring program has been supported by the Australian Research Council (Discovery and Linkage), Northern

Beaches Council, SIMS Foundation and NSW Department of Planning, Industry and Environment (NSW DPIE). High-resolution topographic data was collected by Nashwan Matheen, Chris Leaman, Raimundo Ibaceta and Tom Beuzen. Wave and tide data at Narrabeen-Collaroy were kindly provided by the Manly Hydraulics Laboratory on behalf of NSW DPIE. The authors would like to thank the United States Army Corps of Engineers Field Research Facility at Duck, North Carolina for making their data publicly available via the CHL THREDDS data server (https://chlthredds.erdc.dren.mil/thredds/catalog/frf/catalog.html).

## *References*

Adebisi, N., Balogun, A.-L., Mahdianpari, M., Min, T.H., 2021. Assessing the Impacts of Rising Sea Level on Coastal Morpho-Dynamics with Automated High-Frequency Shoreline Mapping Using Multi-Sensor Optical Satellites. Remote Sens. 13, 3587. https://doi.org/10.3390/rs13183587

Almeida, L.P., Efraim de Oliveira, I., Lyra, R., Scaranto Dazzi, R.L., Martins, V.G., Henrique da Fontoura Klein, A., 2021. Coastal Analyst System from Space Imagery Engine (CASSIE): Shoreline management module. Environ. Model. Softw. 140, 105033. https://doi.org/10.1016/j.envsoft.2021.105033

Almonacid-Caballer, J., Sánchez-García, E., Pardo-Pascual, J.E., Balaguer-Beser, A.A., Palomar-Vázquez, J., 2016. Evaluation of annual mean shoreline position deduced from Landsat imagery as a mid-term coastal evolution indicator. Mar. Geol. 372, 79–88. https://doi.org/10.1016/j.margeo.2015.12.015

Belward, A.S., Skøien, J.O., 2015. Who launched what, when and why; trends in global land-cover observation capacity from civilian earth observation satellites. ISPRS J. Photogramm. Remote Sens. 103, 115–128. https://doi.org/10.1016/j.isprsjprs.2014.03.009

Boak, E.H., Turner, I.L., 2005. Shoreline Definition and Detection: A Review. J. Coast. Res. 214, 688–703. https://doi.org/10.2112/03-0071.1

Bracs, M.A., Turner, I.L., Splinter, K.D., Short, A.D., Lane, C., Davidson, M.A., Goodwin, I.D., Pritchard, T., Cameron, D., 2016. Evaluation of Opportunistic Shoreline Monitoring Capability Utilizing Existing "Surfcam" Infrastructure. J. Coast. Res. 319, 542–554. https://doi.org/10.2112/JCOASTRES-D-14-00090.1

Castelle, B., Masselink, G., Scott, T., Stokes, C., Konstantinou, A., Marieu, V., Bujan, S., 2021. Satellite-derived shoreline detection at a high-energy meso-macrotidal beach.

Geomorphology 383, 107707. https://doi.org/10.1016/j.geomorph.2021.107707

Chander, G., Markham, B.L., Helder, D.L., 2009. Summary of current radiometric calibration coefficients for Landsat MSS, TM, ETM+, and EO-1 ALI sensors. Remote Sens. Environ. 113, 893–903. https://doi.org/10.1016/j.rse.2009.01.007

Cipolletti, M.P., Delrieux, C.A., Perillo, G.M.E., Cintia Piccolo, M., 2012. Superresolution border segmentation and measurement in remote sensing images. Comput. Geosci. 40, 87–96. https://doi.org/10.1016/j.cageo.2011.07.015

Cuttler, M.V.W., Vos, K., Branson, P., Hansen, J.E., O'Leary, M., Browne, N.K., Lowe, R.J., 2020. Interannual Response of Reef Islands to Climate-Driven Variations in Water Level and Wave Climate. Remote Sens. 12, 4089. https://doi.org/10.3390/rs12244089

Dewi, R.S., 2019. Monitoring long-term shoreline changes along the coast of Semarang. IOP Conf. Ser. Earth Environ. Sci. 284. https://doi.org/10.1088/1755-1315/284/1/012035

Dobrinić, D., Gašparović, M., Župan, R., 2018. Horizontal accuracy assessment of planetscope, rapideye and worldview-2 satellite imagery. Int. Multidiscip. Sci. GeoConference Surv. Geol. Min. Ecol. Manag. SGEM 18, 129–136. https://doi.org/10.5593/sgem2018/2.3/S10.017

Duarte, C.R., de Miranda, F.P., Landau, L., Souto, M.V.S., Sabadia, J.A.B., Neto, C.Â. da S., Rodrigues, L.I. de C., Damasceno, A.M., 2018. Short-time analysis of shoreline based on RapidEye satellite images in the terminal area of Pecém Port, Ceará, Brazil. Int. J. Remote Sens. 39, 4376–4389. https://doi.org/10.1080/01431161.2018.1457229

Emery, K.O., 1961. A simple method of measuring beach profiles. Limnol. Oceanogr. 6, 90–93.

Farris, A.S., List, J.H., 2007. Shoreline Change as a Proxy for Subaerial Beach Volume Change. J. Coast. Res. 233, 740–748. https://doi.org/10.2112/05-0442.1

Fish, M.R., Côté, I.M., Horrocks, J.A., Mulligan, B., Watkinson, A.R., Jones, A.P., 2008. Construction setback regulations and sea-level rise: Mitigating sea turtle nesting beach loss. Ocean Coast. Manag. 51, 330–341. https://doi.org/10.1016/j.ocecoaman.2007.09.002

Ford, M., 2013. Shoreline changes interpreted from multi-temporal aerial photographs and high resolution satellite images: Wotje Atoll, Marshall Islands. Remote Sens. Environ. 135, 130–140. https://doi.org/10.1016/j.rse.2013.03.027

García-Rubio, G., Huntley, D., Russell, P., 2015. Evaluating shoreline identification using optical satellite images. Mar. Geol. 359, 96–105. https://doi.org/10.1016/j.margeo.2014.11.002

Gorelick, N., Hancher, M., Dixon, M., Ilyushchenko, S., Thau, D., Moore, R., 2017. Google Earth Engine: Planetary-scale geospatial analysis for everyone. Remote Sens. Environ. 202, 18–27. https://doi.org/10.1016/j.rse.2017.06.031

Hagenaars, G., de Vries, S., Luijendijk, A.P., de Boer, W.P., Reniers, A.J.H.M., 2018. On the accuracy of automated shoreline detection derived from satellite imagery: A case study of the sand motor mega-scale nourishment. Coast. Eng. 133, 113–125. https://doi.org/10.1016/j.coastaleng.2017.12.011

Harley, M.D., Kinsela, M.A., Sánchez-García, E., Vos, K., 2019. Shoreline change mapping using crowd-sourced smartphone images. Coast. Eng. 150, 175–189. https://doi.org/10.1016/j.coastaleng.2019.04.003

Harley, M.D., Kinsela, M.A., 2022. CoastSnap: A global citizen science program to monitor changing coastlines. Cont. Shelf Res. 245, 104796, https://doi.org/10.1016/j.csr.2022.104796

Harley, M.D., Turner, I.L., Short, A.D., Ranasinghe, R., 2011. Assessment and integration of conventional, RTK-GPS and image-derived beach survey methods for daily to decadal coastal monitoring. Coast. Eng. 58, 194–205.

Harley, M.D., Turner, I.L., Short, A.D., Ranasinghe, R., 2009. An empirical model of beach response to storms -- SE Australia, in: Coasts and Ports 2009: In a Dynamic Environment. Engineers Australia, pp. 600–606.

Holman, R.A., Stanley, J., Özkan-Haller, H.T., 2003. Applying Video Sensor Networks to Nearshore Environmental Monitoring. IEEE Pervasive Comput. 2, 14–21.

Jaud, M., Kervot, M., Delacourt, C., Bertin, S., 2019. Potential of Smartphone SfM Photogrammetry to Measure Coastal Morphodynamics. Remote Sens. 11, 2242. https://doi.org/10.3390/rs11192242

Kelly, J.T., Gontz, A.M., 2019. Rapid Assessment of Shoreline Changes Induced by Tropical Cyclone Oma Using CubeSat Imagery in Southeast Queensland, Australia. J. Coast. Res. 36, 72. https://doi.org/10.2112/jcoastres-d-19-00055.1

Lawson, S.K., Tanaka, H., Udo, K., Hiep, N.T., Tinh, N.X., 2021. Morphodynamics and Evolution of Estuarine Sandspits along the Bight of Benin Coast, West Africa. Water 13, 2977. https://doi.org/10.3390/w13212977

Lemajic, S., Vajsova, B., Åstrand, P.J., 2017. New sensors benchmark report on PlanetScope, Joint Research Centre. https://doi.org/10.2760/178918

Liu, Q., Trinder, J., Turner, I.L., 2017. Automatic super-resolution shoreline change monitoring using Landsat archival data: a case study at Narrabeen–Collaroy Beach,

Australia. J. Appl. Remote Sens. 11, 016036. https://doi.org/10.1117/1.JRS.11.016036

Luijendijk, A., Hagenaars, G., Ranasinghe, R., Baart, F., Donchyts, G., Aarninkhof, S., 2018. The State of the World's Beaches. Sci. Rep. 8, 1–11. https://doi.org/10.1038/s41598-018-24630-6

Mao, Y., Harris, D.L., Xie, Z., Phinn, S., 2021. Efficient measurement of large-scale decadal shoreline change with increased accuracy in tide-dominated coastal environments with Google Earth Engine. ISPRS J. Photogrammetry and Remote Sens. 118, 385-399, https://doi.org/10.1016/j.isprsjprs.2021.09.021

McFeeters, S.K., 1996. The use of the Normalized Difference Water Index (NDWI) in the delineation of open water features. Int. J. Remote Sens. 17, 1425–1432. https://doi.org/10.1080/01431169608948714

Mentaschi, L., Vousdoukas, M.I., Pekel, J.-F., Voukouvalas, E., Feyen, L., 2018. Global long-term observations of coastal erosion and accretion. Sci. Rep. 8, 12876. https://doi.org/10.1038/s41598-018-30904-w

Moore, L.J., 2000. Shoreline Mapping Techniques. J. Coast. Res. 16, 111–124.

Pardo-Pascual, J., Sánchez-García, E., Almonacid-Caballer, J., Palomar-Vázquez, J., Priego de los Santos, E., Fernández-Sarría, A., Balaguer-Beser, Á., 2018. Assessing the Accuracy of Automatically Extracted Shorelines on Microtidal Beaches from Landsat 7, Landsat 8 and Sentinel-2 Imagery. Remote Sens. 10, 326. https://doi.org/10.3390/rs10020326

Pardo-Pascual, J.E., Almonacid-Caballer, J., Ruiz, L.A., Palomar-Vázquez, J., 2012. Automatic extraction of shorelines from Landsat TM and ETM+ multi-temporal images with subpixel precision. Remote Sens. Environ. 123, 1–11. https://doi.org/10.1016/j.rse.2012.02.024

Pedregosa, F., Varoquaux, G., Gramfort, A., Michel, V., Thirion, B., Grisel, O., Blondel, M., Prettenhofer, P., Weiss, R., Dubourg, V., Vanderplas, J., Passos, A., Cournapeau, D., Brucher, M., Perrot, M., Duchesnay, É., 2011. Scikit-learn: Machine learning in Python. J. Mach. Learn. Res.

Phillips, M. S., Harley, M.D., Turner, I.L., Splinter, K.D., Cox, R.J., 2017. Shoreline recovery on wave-dominated sandy coastlines: the role of sandbar morphodynamics and nearshore wave parameters. Mar. Geo. 385, 146-159, http://dx.doi.org/10.1016/j.margeo.2017.01.005.

Pianca, C., Holman, R., Siegle, E., 2015. Shoreline variability from days to decades: Results of long-term video imaging. J. Geophys. Res. C Ocean. 120, 2159–2178. https://doi.org/10.1002/2014JC010329

Planet, 2020. Planet Imagery Product Specifications June 2020.

Plant, N.G., Stockdon, H.F., 2012. Probabilistic prediction of barrier-island response to hurricanes. J. Geophys. Res. Earth Surf. 117, 1–17. https://doi.org/10.1029/2011JF002326

Pucino, N., Kennedy, D.M., Carvalho, R.C., Allan, B., Ierodiaconou, D., 2021. Citizen science for monitoring seasonal-scale beach erosion and behaviour with aerial drones. Sci. Rep. 11, 3935. https://doi.org/10.1038/s41598-021-83477-6

Romine, B.M., Fletcher, C.H., 2013. A Summary of Historical Shoreline Changes on Beaches of Kauai, Oahu, and Maui, Hawaii. J. Coast. Res. 288, 605–614. https://doi.org/10.2112/JCOASTRES-D-11-00202.1

Silberman, J., Klock, M., 1988. The recreation benefits of beach renourishment. Ocean Shorel. Manag. 11, 73–90. https://doi.org/10.1016/0951-8312(88)90006-9

Splinter, K.D., Harley, M.D., Turner, I.L., 2018. Remote Sensing Is Changing Our View of the Coast : Insights from 40 Years of Monitoring at of. Remote Sens. 10, 1744. https://doi.org/10.3390/rs10111744

Turner, I.L., Harley, M.D., Drummond, C.D., 2016a. UAVs for coastal surveying. Coast. Eng. 114, 19–24. https://doi.org/10.1016/j.coastaleng.2016.03.011

Turner, I.L., Harley, M.D., Short, A.D., Simmons, J.A., Bracs, M.A., Phillips, M.S., Splinter, K.D., 2016b. A multi-decade dataset of monthly beach profile surveys and inshore wave forcing at Narrabeen, Australia. Sci. data 3, 160024. https://doi.org/10.1038/sdata.2016.24

Vos, K., Harley, M.D., Splinter, K.D., Simmons, J.A., Turner, I.L., 2019a. Sub-annual to multi-decadal shoreline variability from publicly available satellite imagery. Coast. Eng. 150, 160–174. https://doi.org/10.1016/j.coastaleng.2019.04.004

Vos, K., Harley, M.D., Splinter, K.D., Walker, A., Turner, I.L., 2020. Beach slopes from satellite-derived shorelines. Geophys. Res. Lett. https://doi.org/10.1029/2020gl088365

Vos, K., Splinter, K.D., Harley, M.D., Simmons, J.A., Turner, I.L., 2019b. CoastSat: A Google Earth Engine-enabled Python toolkit to extract shorelines from publicly available satellite imagery. Environ. Model. Softw. 122, 104528. https://doi.org/10.1016/j.envsoft.2019.104528

Vousdoukas, M.I., Ranasinghe, R., Mentaschi, L., Plomaritis, T.A., Athanasiou, P., Luijendijk, A., Feyen, L., 2020. Sandy coastlines under threat of erosion. Nat. Clim. Chang. 10, 260–263. https://doi.org/10.1038/s41558-020-0697-0

Xu, H. 2006. Modification of normalised difference water index (NDWI) to enhance open

water features in remotely sensed imagery. Int. J. Remote Sens. 27, 3025-3033, https://doi.org/10.1080/01431160600589179

Highlights

- A new toolkit introduced to map shoreline change from PlanetScope cubesat images
- Validation at microtidal sandy beach indicates horizontal accuracy of 3.5m
- Capable of mapping shoreline change from individual storm events

**Declaration of interests**

☒ The authors declare that they have no known competing financial interests or personal relationships that could have appeared to influence the work reported in this paper.

☐ The authors declare the following financial interests/personal relationships which may be considered as potential competing interests: